TWO-PHASE FLOW CHARACTERISTICS OF AN UNSTEADY DAM BREAK WAVE FLOW

Hubert CHANSON
Dept of Civil Engineering, The University of Queensland, Brisbane QLD 4072, Australia
Ph.: (61 7) 33 65 43 63 - Fax: (61 7) 33 65 45 99 - E-mail: h.chanson@mailbox.uq.edu.au

Abstract : Although field observations of sudden spillway releases highlighted strong aeration of dam break wave flows, no study investigated these two-phase flow characteristics. New original experiments were conducted down a 24 m long stepped waterways. Dam break wave propagation showed an equivalent flow resistance similar to steady flow conditions ($f \sim 0.05$). Detailed unsteady air-water flow measurements demonstrated very strong aeration of the wave leading edge : $C_{mean} \sim 0.8$ down to 0.4 for $(t - t_s)*\sqrt{g/d_o} < 1.2$ while the air-water flow structure was very coarse. Void fraction distributions compared well with analytical models.

Keywords: dam break wave, unsteady two-phase flows, flash flood, air entrainment.

INTRODUCTION

While there have been detailed studies of dam break waves (e.g. RITTER 1892, HUNT 1982), less attention was paid to flash floods down stormwater systems and flood wave resulting from sudden spillway releases (e.g. Fig. 1). Visual observations suggest strong energy dissipation associated with chaotic flow motion and strong aeration ('white waters') of the wave front (Fig. 1 and 2). How important are these processes ?

In the present study, flood releases down a stepped storm waterway were investigated in a large size facility under controlled flow conditions. Unsteady two-phase flow measurements were conducted in the wave front. The results provide new information on the rate of energy dissipation, downstream wave celerity and flow aeration. It is the purpose of the study to develop new compelling conclusions regarding the propagation of flash floods.

EXPERIMENTAL FACILITIES

Experiments were performed in a 24 m long 0.5 m wide flume with a flat stepped invert (Fig. 2, Table 1). The flow rate was delivered by a pump controlled with an adjustable frequency AC motor drive Taian T-Verter K1/N1 (Pulse Width Modulated design) enabling an accurate discharge adjustment in a closed-circuit system. The flow was fed through a smooth convergent nozzle (1.7-m long). The nozzle exit was 30-mm high and 0.5-m wide and the measured contraction ratio was about unity. The flow rates in steady flow conditions were measured with a Dall™ tube flowmeter, calibrated on site. The accuracy on the discharge measurement was about 2%. Prior to the start of each experiment, the recirculation pipe system and convergent intake were emptied. The channel was initially dry. The pump was rapidly started and reached its nominal power (i.e. flow rate) at least 10 seconds prior to water entering the channel. The flow rate Q(t=0+) was maintained constant until the wave front reached the downstream end of the flume. The time origin (t = 0) was taken as the instant when water entered the flume.

Two stepped configurations were used (Table 1). The first geometry was equipped with ten identical steps (0.143-m high 2.4-m long) (Fig. 2). In the second configuration, the nozzle

was followed by a 2.4 m long horizontal invert and by 18 steps (h = 0.0715 m, l = 1.2 m) (Fig. 3). The surging flow was studied with two video-cameras : i.e., VHS video-camera Panasonic™ NV-RX10A (25 fr/sec., shutter: sport mode) and digital video-camera handycam Sony™ DV-CCD DCR-TRV900 (speed: 25 fr/sec., shutter: 1/4 to 1/10,000 sec.). The cameras were installed above and along the axis of the channel. Studies of individual steps were conducted by mounting a camera directly above the step. In experiments Series 1, each result was the average of two identical runs. In Series 2, each data was an average of three runs.

Fig. 1 (Left) - Flood wave down Brushes Clough dam spillway during field tests in 1994 (Courtesy of Dr R. BAKER) - Fig. 2 (Right) - Advancing flood wave down the stepped chute looking upstream ($Q(t=0+) = 0.075$ m^3/s, $h = 0.143$ m)

Fig. 3 - Wave front immediately upstream of the conductivity probes ($Q(t=0+) = 0.055$ m^3/s, $h = 0.07$ m) - Flow from top left to bottom right

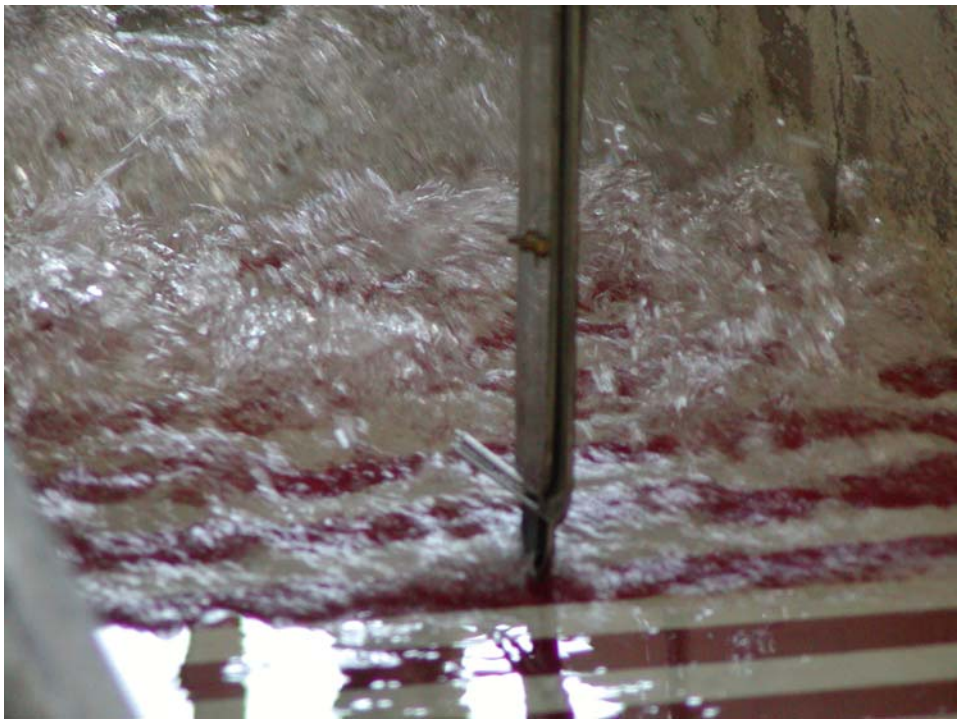

Air-water flow properties were measured with an array of single-tip conductivity probes located on the channel centreline (Fig. 3). Each probe consisted of a sharpened rod (∅ = 0.35 mm) which was insulated except for its tip and set into a metal supporting tube. It was excited by an electronics designed with a response time of less than 10 μs The probe outputs were scanned at 10 kHz per channel for six seconds. One probe (reference probe) was set on the invert acting as time reference, while other probes were set at different vertical elevations (Fig. 3). The vertical displacement of the probes was controlled by a fine adjustment travelling mechanism with an accuracy of 0.2 mm. Further details on the study were reported in CHANSON (2003). Previously, steady flow experiments were conducted in the same channel by CHANSON and TOOMBES (1997, 2002a) and these provide limiting conditions for the present unsteady flow experiments.

Table 1 - Summary of experimental conditions

Run	θ (deg.)	h m	Run	Q(t=0+) (m^3/s)	Steady flow regime	Remarks
(1)	(2)	(3)	(4)	(5)	(6)	(7)
Series 1	3.4	0.143				10 horizontal steps (l = 2.4 m). W = 0.5 m (CHANSON 2001).
			CT15	0.019	Nappe NA3	
			CT26	0.030	Nappe NA3	
			CT37	0.040	Nappe NA3	
			CT48	0.075	Nappe NA3	
Series 2	3.4	0.071				18 horizontal steps (l = 1.2 m).
			TL1	0.040	Transition	Air-water flow measurements.
			TL2	0.0475	Trans./Skim.	
			TL3	0.055	Skimming	Air-water flow measurements.
			TL4	0.065	Skimming	
			TL5	0.075	Skimming	Air-water flow measurements.

Notes : h : step height; l : step length; Q(t=0+) : initial flow rate; W :chute width.

FLOW PATTERNS AND WAVE FRONT PROPAGATION

Visual observations showed that the wave front propagated as a nappe flow. For comparison, the flow regime observations in steady flows are summarised in Table 1 (column 6). Basically the wave front propagated as a succession of free-falling nappe, nappe impact and horizontal runoff at each step for all flow rates and geometries, although steady flow conditions could correspond to nappe, transition or skimming flow regimes as defined by CHANSON (2001). Further the wave front was highly aerated, in particular for the larger flow rates. Figures 2 and 3 highlight the chaotic nature of the flow with strong spray, splashing and wavelets. Visually the wave front had a similar appearance to that observed during prototype tests (Fig. 1).

The propagation of the wave front was recorded. Dimensionless locations of wave front x_s/d_o are presented in Figure 4 as a function of the dimensionless time $t^*\sqrt{g/d_o}$, where x_s is the distance along the pseudo-bottom formed by the step edges measured from the upstream end and d_o is a measure of the initial flow rate Q(t=0+) :

Fig. 4 - Dimensionless wave front location x_s/d_o and wave front celerity $C_s/\sqrt{g*d_o}$ (Q(t=0+) = 0.075 m^3/s, h = 0.07 & 0.143 m) - Comparison with HUNT's (1982) theory

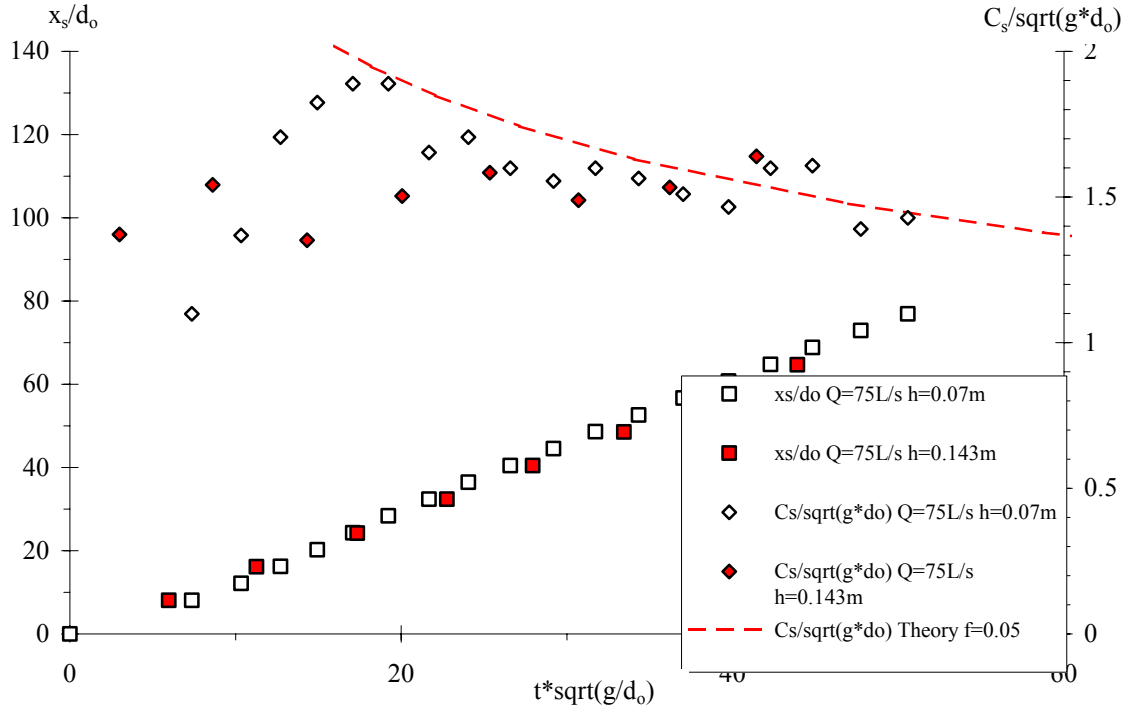

$$d_o = \frac{9}{4} * \sqrt[3]{\frac{Q(t=0+)^2}{g * W^2}} \qquad (1)$$

where W is the channel width. For an ideal dam break, d_o would be equivalent to the initial water depth behind the dam and Q(t=0+) would be the discharge at the origin where critical flow conditions occur. In Figure 4, dimensionless wave front celerity data $C_s/\sqrt{g*d_o}$ are also presented. These were averaged over one step length and measured from one step edge to the next one. For small flow rates (Q(t=0+) ≤ 0.04 m^3/s), the wave front celerity was relatively

uniform along the 24-m long chute. For larger discharges, the flow accelerated in the first 4 to 6 steps. Further downstream, a very-gradual celerity decay was observed (Fig. 4). In average, the dimensionless wave front celerity at the end of the chute was about $C_S/\sqrt{g*d_O} \approx 1.5$ for all flow rates and stepped geometries. The data were compared HUNT's (1982) theory. The latter is valid only after the wave front travels more than 4 times the reservoir length : i.e., $t*\sqrt{g/d_O} \geq 35$. A fair agreement between HUNT's theory and present data was achieved assuming an equivalent Darcy-Weisbach friction factor f = 0.05, irrespective of flow rates and chute configurations. Calculated wave celerity (HUNT 1982) are reported in Figure 4. For comparison, steady flow experiments in the same facility yielded f ~ 0.045 to 0.05 (CHANSON and TOOMBES 2002a).

Although Figure 4 suggests an almost linear relationship between wave front location and time, the wave propagation along each step consisted of nappe take-off at the upstream step edge, free-falling jet, nappe impact and horizontal runoff toward the downstream end of the step. Dimensionless wave front celerity data $C_S/\sqrt{g*d_O}$ along a single step are presented in Figure 5. In the free-jet, C_S is the wave celerity magnitude: $C_S = \sqrt{(C_S)_X{}^2 + (C_S)_Z{}^2}$, where the subscripts x and z refer to the horizontal and vertical celerity components respectively. For all flow rates and step locations, experimental data highlighted nappe acceleration in the free-jet and a slow flow deceleration downstream of nappe impact (Fig. 5). In the free-jet, the celerity data agreed well with simple trajectory equations.

Fig. 5 - Dimensionless wave front celerity along one step length (Step 10, h=0.07 m)

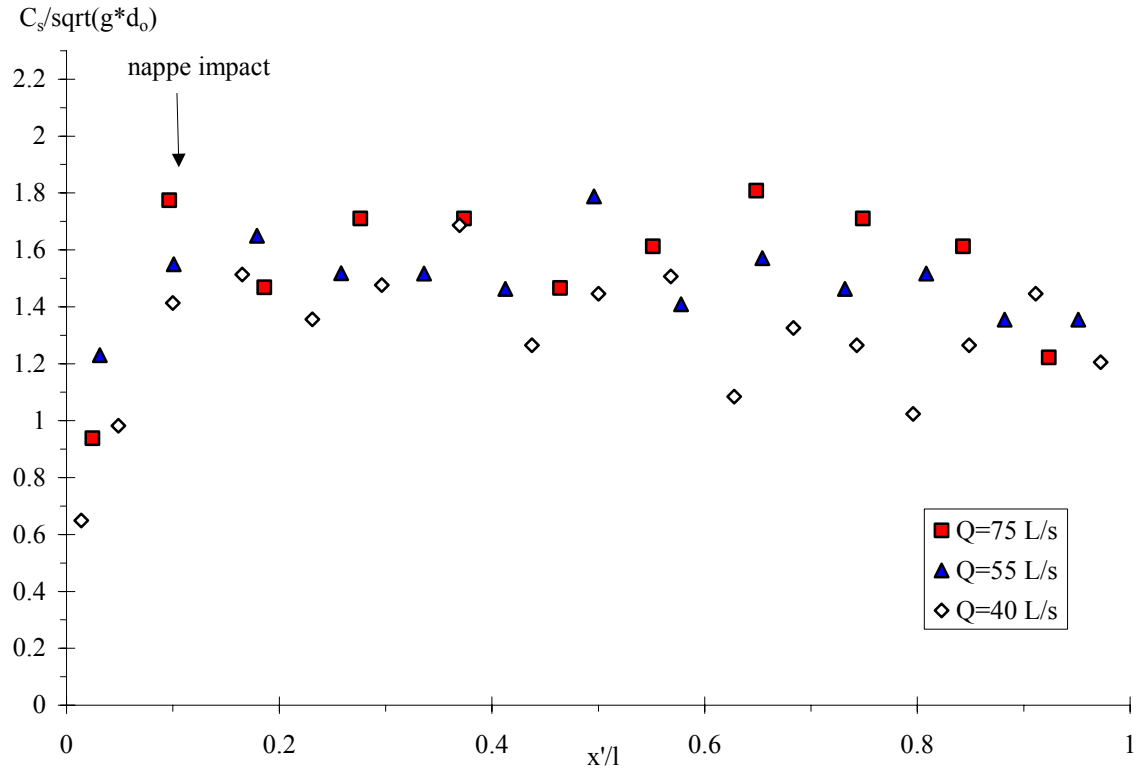

UNSTEADY AIR-WATER FLOW PROPERTIES

In steady flow, the void fraction C is the proportion of time that the probe tip is in the air. In unsteady gas-liquid flows, the processing technique must be adapted. Few studies considered

highly unstationary gas-liquid flows (e.g. STUTZ and REBOUD 2000). In the present work, air concentrations and bubble counts were measured for three flow rates and two steps (Table 1). On each step, void fraction and bubble count distributions were recorded at distances x' = 0.2, 0.4, 0.6, 0.8 and 1.0 m from the vertical step edge (Fig. 6 Insert). A typical example is presented in Figure 6 where void fractions were calculated during a short time interval τ such as $\tau = \Delta x/C_s$ where C_s is the measured surge front celerity and Δx is the control volume streamwise length. In Figure 6, results are presented for Δx = 70, 210 and 385 mm. The legend indicates the control volume location behind the leading edge of wave front: e.g., 0-385 mm means the first 385 mm behind the leading edge. Data for Δx = 0-70 mm, 0-210 mm, 0-385 mm and 700-1085 mm correspond respectively to dimensionless times $(t-t_s)*\sqrt{g/d_o}$ = 0.083, 0.248, 0.455 and 2.11, where t_s is the time of passage of wave front. They are compared with corresponding steady flow data (CHANSON and TOOMBES 2002a).

The distributions of void fractions (Fig. 6) demonstrated a very strong aeration of the leading edge, especially the first 0.3 m of the flow (i.e. $(t-t_s)*\sqrt{g/d_o} < 0.5$). For example, in Figure 6, the depth-average void fractions defined between 0 and 90% were C_{mean} = 0.77, 0.43, 0.45 and 0.31 for Δx = 0-70 mm, 0-210 mm, 0-385 mm and 700-1085 mm respectively. In steady flow, the mean air content was C_{mean} = 0.24 for Q = 0.075 m^3/s, step 16 and x' = 0.8 m. In front of the wave, the void fraction distributions had roughly a linear shape :

$$C = 0.9 * \frac{y}{Y_{90}} \qquad 0.1 < (t - t_s)*\sqrt{g/d_o} < 1.2 \quad (2)$$

where Y_{90} is the location where C = 90%. Equation (2) is a limiting case of the analytical solution of air bubble diffusion equation for steady transition flows down stepped chute (CHANSON and TOOMBES 2002n). For larger times $(t-t_s)$, the distribution of air concentration may be described by a diffusion model developed for steady flows :

$$C = 1 - \tanh^2\left(K'' - \frac{\frac{y}{Y_{90}}}{2 * D_o} + \frac{\left(\frac{y}{Y_{90}} - \frac{1}{3}\right)^3}{3 * D_o}\right) \qquad (t - t_s)*\sqrt{g/d_o} > 1.3 \quad (3)$$

where K' and D_o are functions of the mean air content only (CHANSON and TOOMBES 2002b). Equations (2) and (3) are compared with data in Figure 6. The marked change in void fraction distributions might be attributed to non-hydrostatic pressure distributions and different air-water flow regime (plug/slug flow) at the leading edge (CHANSON 2003).

Fig. 6 - Void fraction C behind the leading edge of wave front (Q(t=0+) = 0.075 m^3/s, h = 0.07 m, Step 16, C_s = 2.43 m/s, x' = 0.8 m) - Comparison with steady flow data (CHANSON and TOOMBES 2002), and Equations (2) and (3)

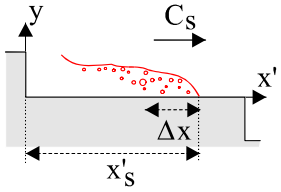

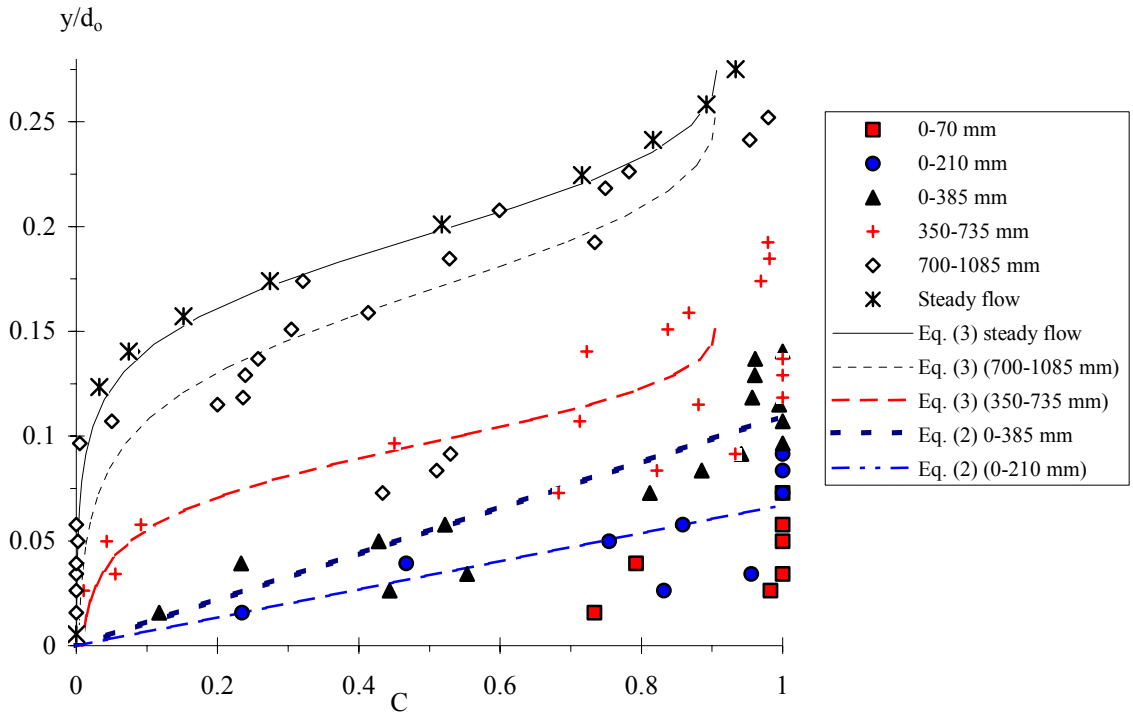

Fig. 7 - Bubble chord size distributions at the leading edge of wave front (Q(t=0+) = 0.075 m^3/s, h = 0.07 m, Step 16, C_S = 2.43 m/s, x' = 1.0 m)

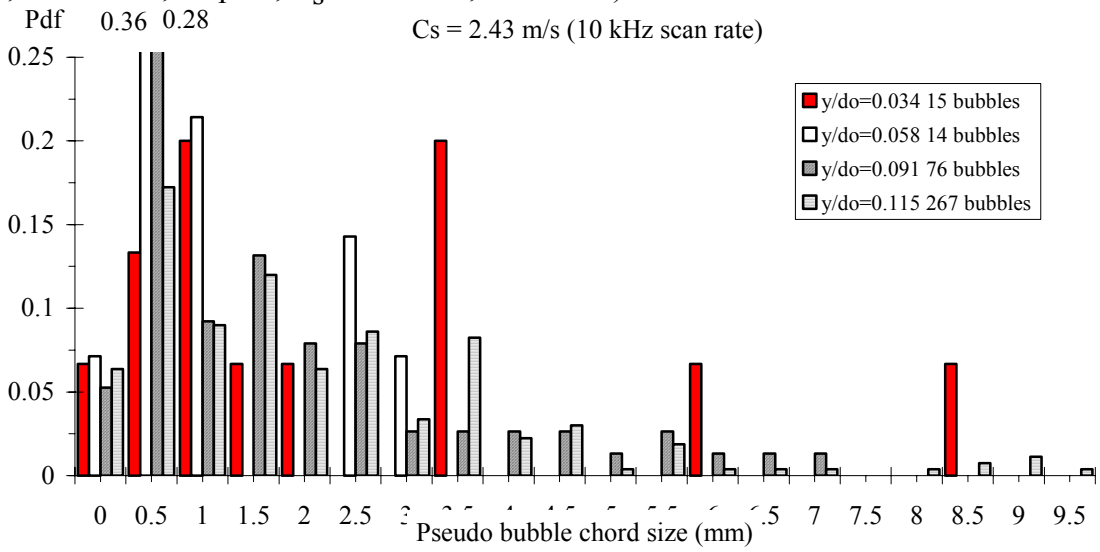

BUBBLE CHORD TIME DISTRIBUTIONS

The bubble chord time t_{ch} is defined as the time spent by the bubble on the probe tip. Bubble and water chord times were measured. The results are presented in terms of pseudo-chord length ch defined as :

$$ch = C_S * t_{ch} \quad (4)$$

where C_S is the wave front celerity. Equation (4) predicts accurately chord lengths near the front where the flow velocity is about the wave front speed. The chord time data analysis was conducted for all the recording, and it was independent of the selection of the integration time interval τ. Pseudo-bubble chord length distribution results are shown in Figure 7. In Figure 7, each histogram shows the normalised probability distribution function of pseudo-bubble

chord length ch_{ab} where the histogram columns represent the probability of chord length in 0.5 mm intervals : e.g., the probability of a chord length from 1.0 to 1.5 mm is represented by the column labelled 1.0. The probability of chord lengths exceeding 10 mm are not shown. For all flow rates and step locations, the data demonstrated a broad spectrum of pseudo-bubble chord lengths from less than 0.5 mm to larger than 20 mm (Fig. 7). The pseudo-bubble chord length distributions were skewed with a preponderance of small bubble sizes relative to the mean. The results highlighted mean pseudo-bubble chord sizes between 3 and 10 mm for $y/d_o < 0.1$. That is, there was a predominance of millimetric entrained bubbles for all flow conditions.

Immediately behind the wave front leading edge, the air-water flow structure consisted of large air packets and water structures entangled together, associated with strong aeration (Fig. 6). In Figure 7 and for $y/d_o = 0.034$, more than half of bubbles were detected for $(t-t_s)*\sqrt{g/d_o} < 0.08$ (Δx = 0-100 mm) with mean bubble chord size of about 6.4 mm.

SUMMARY AND CONCLUSIONS

Detailed measurements were conducted in unsteady dam break wave flows down a stepped waterway with two step heights (θ = 3.4º, 24 m length, 0.5 m width). Visual observations highlighted the chaotic nature of wave front. The leading edge of the flow was a succession of free-falling jet at each brink followed by nappe impact and horizontal runoff. The wave front celerity data were reasonably well predicted by HUNT's (1982) theory assuming an equivalent Darcy friction factor f = 0.05 irrespective of flow rates and chute configurations. Above one step length, experimental data highlighted nappe acceleration in the free-jet and a slow flow deceleration downstream of nappe impact for all flow rates and steps.

New unsteady air-water flow measurements demonstrated very-strong aeration of the leading edge of wave front. For $0.1 < (t - t_s)*\sqrt{g/d_o} < 1.2$, void fraction distributions had a nearly linear shape, while the air concentration distributions had a shape similar to steady flow conditions (Eq. (3)) for larger times (Fig. 6). Distributions of pseudo-bubble chord sizes exhibited a broad range from less than 0.5 mm to more than 20 mm, with mean chords between 3 and 10 mm for $y/d_o < 0.1$. At the leading edge of wave front, the air-water structure was coarse while the mean air content ranged from 0.8 down to 0.4 for $(t-t_s)*\sqrt{g/d_o} < 1.2$.

The strong aeration of the leading edge of the wave front has implications in terms of mass transfer and flow bulking. The enhanced air-water interface area enhances re-oxygenation, which in turn may attenuate water pollution induced by debris and hydrocarbons trapped in front of the wave. The aeration of the flow increases the wave height, and in turn the height of the sidewall. Note further that the aeration of the leading edge will reduce buoyancy (i.e. flotation) in that region, particularly for solid particles smaller than the "air bubble" structures. Such solid debris are more likely to roll than to be suspended.

ACKNOWLEDGMENTS

The writer thanks his students Chung-hwee Jerry LIM and York-wee TAN for their help and assistance.

REFERENCES

CHANSON, H. (2001). "The Hydraulics of Stepped Chutes and Spillways." *Balkema*, Lisse, The Netherlands, 418 pages.

CHANSON, H. (2003). "Sudden Flood Release down a Stepped Cascade." *Report CH51/03*, Dept of Civil Eng., Univ. of Queensland, Brisbane, Australia.

CHANSON, H., and TOOMBES, L. (1997). "Energy Dissipation in Stepped Waterway." *Proc. 27th IAHR Congress*, San Francisco, USA, Vol. D, F.M. HOLLY Jr. and A. ALSAFFAR Ed., pp. 595-600.

CHANSON, H., and TOOMBES, L. (2002a). "Energy Dissipation and Air Entrainment in a Stepped Storm Waterway: an Experimental Study." *Jl of Irrigation and Drainage Engrg.*, ASCE, Vol. 128, No. 5, pp. 305-315.

CHANSON, H., and TOOMBES, L. (2002b). "Experimental Investigations of Air Entrainment in Transition and Skimming Flows down a Stepped Chute." *Can. Jl of Civil Eng.*, Vol. 29, No. 1, pp. 145-156.

HUNT, B. (1982). "Asymptotic Solution for Dam-Break Problems." *Jl of Hyd. Div.*, Proceedings, ASCE, Vol. 108, No. HY1, pp. 115-126.

RITTER, A. (1892). "Die Fortpflanzung der Wasserwellen." *Vereine Deutscher Ingenieure Zeitswchrift*, Vol. 36, No. 2, 33, 13 Aug., pp. 947-954 (in German).

STUTZ, B., and REBOUD, J.L. (2000). "Measurements within Unsteady Cavitation." *Experiments in Fluids*, Vol. 29, pp. 545-552.